IEEE Access
Multidisciplinary | Rapid Review | Open Access Journal

Received September 16, 2020, accepted September 24, 2020, date of publication September 28, 2020,
date of current version November 3, 2020.

Digital Object Identifier 10.1109/ACCESS.2020.3027365

Secure Wireless Transmission for Intelligent Reflecting Surface-Aided Millimeter-Wave Systems

YUE XIU AND ZHONGPEI ZHANG
National Key Laboratory of Science and Technology on Communications, University of Electronic Science and Technology of China, Chengdu 611731, China
Corresponding author: Zhongpei Zhang (zhangzp@uestc.edu.cn)

This work was supported in part by the Guangdong Province Key Project of Science and Technology under Grant 2018B010115001.

ABSTRACT Due to the broadcast nature of millimeter wave (mmWave) communications, physical layer security has always been a fundamental but challenging concern. Fortunately, the recent advance of intelligent reflecting surface (IRS) introduces another dimension for mmWave secure communications by reconfiguring the transmission environments. In this article, we investigate the physical layer security issue for IRS-aided mmWave communications. Specifically, two scenarios are considered, i.e., with and without the knowledge of the eavesdropper's channel. When the eavesdropper's channel is known, under the unit modulus constraints at the IRS and the transmit power constraint at the access point (AP), the secrecy rate is maximized by jointly designing the beamforming vector of the AP and the phase shifts of the IRS. We propose an alternating optimization algorithm for improving the secrecy rate to solve the non-convex optimization problem. In particular, the phase shift matrix of the IRS is firstly optimized based on the manifold optimization algorithm. Under the given phase shift matrix of the IRS, the original problem is transformed into a difference of convex (DC) programming problem. To solve this problem, we use the successive convex approximation (SCA)-based method to transform the original problem into a convex approximation problem, and the transmit beamforming vector is obtained by solving the convex approximation problem. In addition, when the eavesdropper's channel is unknown, under the transmit power constraint and the minimum user rate constraint, an artificial-noise (AN)-aided scheme is proposed to jam the eavesdropper by maximizing the AN power. Numerical results evaluate that the performance of our proposed schemes is better than that of the conventional scheme in terms of secrecy rate. Moreover, simulations also demonstrate that the secrecy behaviors of the IRS-aided mmWave communication system are superior to the mmWave communications without IRS.

INDEX TERMS Intelligent reflecting surface, millimeter wave, manifold optimization, successive convex approximation, artificial-noise.

I. INTRODUCTION

Intelligent reflecting surface (IRS) has recently attracted a lot of research interests from academia as one candidate technology for the fifth-generation (5G) cellular networks [1], [6], [8]. An IRS consists of many reflecting elements whose reflecting phase shifts can adaptively adjust to change the signal propagation environment for improving the rate of the communication system. For instance, the IRS can adequately reflect the signals sent from the access point (AP) towards desirable directions, to efficiently enhance received signal power at intended users and suppress interference at unintended users. Furthermore, the IRS is passive antenna arrays with significantly reduced energy consumption. Based on the above-mentioned advantages of the IRS, IRS technology has been extensively applied in many communication scenarios recently [9]–[15].

The associate editor coordinating the review of this manuscript and approving it for publication was Pietro Savazzi.

A. RELATED WORK

Recently, there is a lot of literature on the design and optimization of IRS-aided wireless systems [1]–[7]. [1] provided an overview of the IRS-aided wireless systems, including the applications, hardware structure, beamforming optimization, channel state information (CSI)

acquisition, and network deployment. In [2], to maximize the received signal-to-noise ratio (SNR) for an IRS-aided single-user multiple-input single-output (MISO) system, the phase shift of IRS and transmit beamforming are jointly optimized. In [3], under minimum user rate constraints, the minimization power problem of IRS-aided MISO systems was investigated.

In [4] and [5], an alternating optimization algorithm for achieving higher energy efficiency and sum-rate was proposed by joint allocating the user's power and designing the phase shift matrix at the IRS. In [6] and [7], compared with the above works, these works took into account the IRS with discrete phase shits instead of the IRS with continuous phase shifts, IRS with discrete phase shifts was investigated for MISO systems with a single user and multiple users. In IRS-aided systems with wireless networks, in addition to sum-rate optimization of systems addressed in above these papers, many other problems have also been investigated in the literature, including information rate maximization in [14], [16]–[21], channel estimation in [15], [36], and positioning in [37], [37], [38]. To summarize, these studies show that the IRS is beneficial for enhancing the performance of various wireless communication systems, e.g., sum-rate, channel estimation accuracy, and energy efficiency. However, to the best of our knowledge, in these works, the optimization problem of the secrecy rate of IRS-aided mmWave communication systems rarely is investigated, which is a vital issue for mmWave communication systems.

Recently, some efforts have been made to study the IRS-aided system for physical layer security. In [22], [23], [28], the problem of maximizing the secrecy rate in an IRS-aided secure MISO communication system is investigated. An alternate optimization strategy was proposed to optimize the transmit beamforming vector at the BS and the phase shifts at the IRS. In [25], the authors investigated the secure communication problem of an IRS-aided MISO system with a single user and a single eavesdropper, but it was limited to a special scenario, where the two channels from BS to eavesdropper and user are highly correlated. Similarly, in [27], the authors considered a secure IRS-aided downlink MISO broadcast system, and the channels from BS to eavesdropper and user are also highly correlated. In [24], the transmission design for an IRS-aided secure MISO communication is considered, in which the system energy consumption is minimized under two assumptions that the channels of the access point (AP)-IRS links are rank-one and full-rank. In [29], the authors investigated the physical layer security in an IRS-aided simultaneous wireless information and power transfer (SWIPT) system. Moreover, there are some papers considering the IRS-assisted secure communication with AN. In [30], the authors considered a secure IRS-aided MISO communication system, the beamforming vector, and the IRS phase shifts were optimized to jam the eavesdropper. In [26], the resource allocation problem in an IRS-aided MISO system by jointly optimizing the beamforming vector, the phase shifts of the IRS, and AN power for secrecy rate maximization. In [31], the authors further considered AN in an IRS-aided MIMO system by jointly optimizing the phase shifts of the IRS, and the AN power to jam the eavesdropper.

Although a few papers have studied security enhancement for an IRS-aided system, the above-mentioned existing papers related to this topic either only studied the microwave scenario or assumed special settings to the channels. The investigation on the mmWave scenario with general channel settings is absent in the above-mentioned literature. Moreover, although [32] studied the security of IRS-aided mmWave communication systems and [33] studied the robust security of IRS-aided mmWave communication systems, these studies only considered partial perfect CSI. The physical layer security of the IRS-aided mmWave communication system when the eavesdropper's CSI is completely unknown has not yet been studied. Therefore, we investigate this physical layer security problem of an IRS-aided mmWave MISO communication system for the known eavesdropper's CSI and the unknown eavesdropper's CSI.

B. CONTRIBUTION

We focus on the secure beamforming design of an IRS-aided mmWave system with an eavesdropper in this article. Our contributions can be summarized as follows:

- When the channel of the eavesdropper is perfectly known, under the transmit power constraints of the access point (AP) and unit-modulus constraint, our objective is to maximize the secrecy rate. However, the non-convexity of unit-modulus constraints of the IRS renders the considered problem very difficult to solve. As such, we propose an alternating optimization algorithm. Specifically, we design the phase shift matrix of the IRS by resorting to the manifold optimization technique while the transmit beamforming vector is considered as a known parameter. Given the obtained phase shift matrix, the original optimization problem is reformulated as a difference of convex (DC) programming. Then we propose a successive convex approximation (SCA)-based algorithm to solve it.
- When the channel of the eavesdropper is unknown, to jam the eavesdropper, we introduce an artificial noise (AN). Under the transmit power constraints, by maximizing the AN power to restrain the eavesdropper.
- Finally, what is presented by simulation results is that IRS is capable of upgrading the secrecy rate of mmWave greatly, but a point that can not be neglected is the phase shift of the IRS has to be designed reasonably. Simulation results also show that more transmit power is beneficial to security. Moreover, to realize the full potential of the IRS, it is important to select the IRS location.

Organization: The rest of the paper is organized as follows. We describe the system model and problem formulation in Section II. In Section III, we propose an alternating optimization algorithm for the secure beamforming problem and

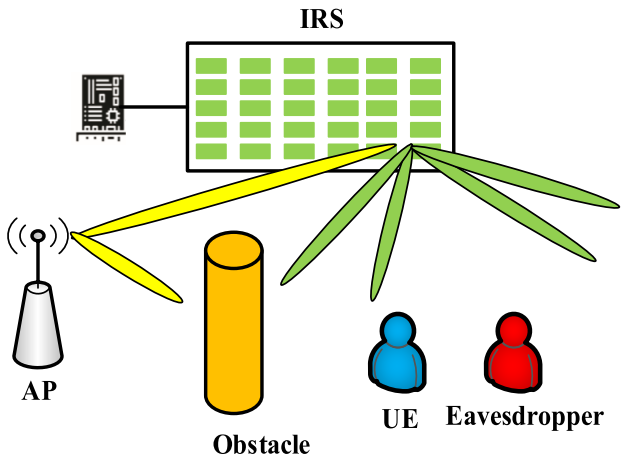

FIGURE 1. System model for IRS-aided mmWave communication system with eavesdropper.

also give an AN-based scheme for without eavesdropper's channel. In Section IV, numerical simulations are provided to show the algorithm efficiency and the secrecy rate enhancement. Section V concludes this article.

Notations: Vectors and matrices are denoted as boldface lowercase, and uppercase letters, respectively. The transpose, conjugate, conjugate transpose, Frobenius norm, and trace of the matrix $\boldsymbol{X}$ are denoted $\boldsymbol{X}^T$, $\boldsymbol{X}^*$, $\boldsymbol{X}^H$, $\|\boldsymbol{X}\|$, and $\mathrm{tr}(\boldsymbol{X})$, respectively. The $\odot$ is Hadamard product. The $\mathrm{vec}(\boldsymbol{X})$ denotes to stack the columns of the matrix $\boldsymbol{X}$ into a single vector. Let $\mathrm{Re}\{a\}$ be the real part of a complex variable a. The positive semidefinite and positive definite of the matrix $\boldsymbol{X}$ are denoted as $\boldsymbol{X} \succeq \boldsymbol{0}$ and $\boldsymbol{X} \succ \boldsymbol{0}$, respectively.

II. SYSTEM MODEL AND PROBLEM FORMULATION

As shown in Fig.1, we consider an IRS-aided mmWave system, which consists of one AP, one IRS, one user and one eavesdropper. The AP and IRS are respectively equipped with N_t antennas and N_r reflecting elements. The user and eavesdropper are each equipped with a single antenna. In this article, it is assumed that the direct link between the AP and the user or eavesdropper is blocked by obstacles [13], [42]. In addition, we assume that the eavesdropper is active, thus the eavesdropper's channel is known at the AP [41].

Denote the AP-to-IRS mmWave channel, the IRS-to-user mmWave channel, and IRS-to-eavesdropper mmWave channel as $\boldsymbol{G}_{AI} \in \mathbb{C}^{N_r \times N_t}$, $\boldsymbol{h}_{IU} \in \mathbb{C}^{N_r \times 1}$, and $\boldsymbol{h}_{IE} \in \mathbb{C}^{N_r \times 1}$, respectively. The received signal at the IRS is expressed as

$$\boldsymbol{r} = \boldsymbol{G}_{AI}\boldsymbol{w}s, \tag{1}$$

where $\boldsymbol{r} \in \mathbb{C}^{N_r \times 1}$. $s \in \mathbb{C}^{1\times 1}$ and $\boldsymbol{w} \in \mathbb{C}^{N_t \times 1}$ denote the transmit data and the transmit beamforming vector at the AP with $\mathbb{E}[ss^H] = 1$; Then, the IRS reflects it with a phase shift matrix $\boldsymbol{\Theta} = \mathrm{diag}(\boldsymbol{\theta}) \in \mathbb{C}^{N_r \times N_r}$, where $\boldsymbol{\theta} = [\theta_1, \cdots, \theta_{N_r}]^T \in \mathbb{C}^{N_r \times 1}$ and $\theta_j = e^{j\phi_j}, j = 1, \cdots, N_r$ with ϕ_j being the reflection phase shift. The received signal at the user can be written as

$$y = \boldsymbol{h}_{IU}^H \boldsymbol{\Theta} \boldsymbol{G}_{AI} \boldsymbol{w} s + n, \tag{2}$$

where n is the additive white Gaussian noise (AWGN) and $n \sim \mathcal{CN}(0, \sigma^2)$. Similarly, the received signal at the eavesdropper is expressed as

$$y_e = \boldsymbol{h}_{IE}^H \boldsymbol{\Theta} \boldsymbol{G}_{AI} \boldsymbol{w} s + n_e, \tag{3}$$

where n_e is also the additive white Gaussian noise (AWGN) and $n_e \sim \mathcal{CN}(0, \sigma_e^2)$.

From (2) and (3), the achievable rate at the user is

$$I = \log_2 \left(1 + \frac{1}{\sigma^2} \left\| \boldsymbol{h}_{IU}^H \boldsymbol{\Theta} \boldsymbol{G}_{AI} \boldsymbol{w} \right\|^2 \right). \tag{4}$$

The achievable rate at the eavesdropper is

$$I_e = \log_2 \left(1 + \frac{1}{\sigma_e^2} \left\| \boldsymbol{h}_{IE}^H \boldsymbol{\Theta} \boldsymbol{G}_{AI} \boldsymbol{w} \right\|^2 \right). \tag{5}$$

Therefore, the secrecy rate I_s is denoted as [22],

$$I_s = [I - I_e]^+, \tag{6}$$

where $[x]^+ = \max(0, x)$. The transmit power constraint at the AP is

$$\mathrm{tr}\left(\boldsymbol{w}\boldsymbol{w}^H\right) \le P, \tag{7}$$

where P is the maximum transmit power at the AP. Based on (6) and (7), the secure beamforming optimization problem for the IRS-aided mmWave system with power constraint is formulated as

$$\begin{aligned} &\max_{\boldsymbol{w}, \boldsymbol{\Theta}} \ I_s, \\ &\text{s.t. } \mathrm{tr}\left(\boldsymbol{w}\boldsymbol{w}^H\right) \le P, \\ &\quad |\theta_j| = 1, j = 1, \cdots, N_r. \end{aligned} \tag{8}$$

Due to the non-convexity of the unit-modulus of the IRS and the objective function, the problem in (8) is non-convex.

III. SECURE BEAMFORMING FOR IRS-AIDED mmWave SYSTEMS

A. JOINT TRANSMIT BEAMFORMING AND PHASE SHIFT OF THE IRS DESIGN WITH FULL EAVESDROPPER's CHANNEL

Since there is no general method to solve the non-convex problem in (8) efficiently and optimally, we develop an alternating optimization algorithm to solve (8) in this article. In the following, an alternating optimization algorithm is proposed to solve this problem. Specifically, first, we optimize the phase shift matrix $\boldsymbol{\Theta}$ by using manifold optimization technology. Then the phase shift matrix $\boldsymbol{\Theta}$ is fixed, we transform the problem in (8) into a DC programming problem [35]. To solve this problem, an SCA-based algorithm is proposed to obtain the local optimal solution of transmit beamforming of the AP.

For resolving the problem in (8), the auxiliary variables $\boldsymbol{x}$ and $v_i, i = 1, 2$ are introduced and they satisfy the following equalities

$$\boldsymbol{x} = \boldsymbol{\Theta} \boldsymbol{G}_{AI} \boldsymbol{w}, \tag{9}$$

$$v_1 = \frac{1}{\sigma^2} \boldsymbol{x}^H \boldsymbol{h}_{IU} \boldsymbol{h}_{IU}^H \boldsymbol{x}, \tag{10}$$

$$v_2 = \frac{1}{\sigma_e^2}\boldsymbol{x}^H\boldsymbol{h}_{IE}\boldsymbol{h}_{IE}^H\boldsymbol{x}. \tag{11}$$

Using (9)-(11), the problem in (8) can be rewritten as

$$\max_{\boldsymbol{w},\boldsymbol{\Theta},\boldsymbol{x},\{v_i\}_{i=1,2}} \ \ln(1+v_2)-\ln(1+v_1), \tag{12a}$$
$$\text{s.t. } \boldsymbol{x} = \boldsymbol{\Theta}\boldsymbol{G}_{AI}\boldsymbol{w}, \tag{12b}$$
$$v_1 = \frac{1}{\sigma^2}\boldsymbol{x}^H\boldsymbol{h}_{IU}\boldsymbol{h}_{IU}^H\boldsymbol{x}, \tag{12c}$$
$$v_2 = \frac{1}{\sigma_e^2}\boldsymbol{x}^H\boldsymbol{h}_{IE}\boldsymbol{h}_{IE}^H\boldsymbol{x}, \tag{12d}$$
$$\text{tr}\left(\boldsymbol{w}\boldsymbol{w}^H\right) \le P, \tag{12e}$$
$$|\theta_n| = 1, n = 1, \cdots, N_r. \tag{12f}$$

In problem (12), since $-\ln(1+v_1)$ is convex, the objective function is the difference of two convex functions. It is not difficult to find that (12e) is convex. Thus, except constraints (12b)-(12d) and (12f), the problem in (12) has a DC form. Now, we deal with these non-convex constraints (12b)-(12d) and have:

Theorem 1: We can equivalently transform constraints (12b), (12c), and (12d) into

$$\begin{bmatrix} v_1 & \boldsymbol{x}^H\boldsymbol{h}_{IU} \\ \boldsymbol{h}_{IU}^H\boldsymbol{x} & \sigma^2\boldsymbol{I} \end{bmatrix} \succeq \boldsymbol{0}, \tag{13}$$
$$\begin{bmatrix} v_2 & \boldsymbol{x}^H\boldsymbol{h}_{IE} \\ \boldsymbol{h}_{IE}^H\boldsymbol{x} & \sigma_e^2\boldsymbol{I} \end{bmatrix} \succeq \boldsymbol{0}, \tag{14}$$
$$\text{tr}\left((\boldsymbol{x}-\boldsymbol{\Theta}\boldsymbol{G}_{AI}\boldsymbol{w})(\boldsymbol{x}-\boldsymbol{\Theta}\boldsymbol{G}_{AI}\boldsymbol{w})^H\right) = 0, \tag{15}$$
$$\text{tr}\left(v_1 - \frac{1}{\sigma^2}\boldsymbol{x}^H\boldsymbol{h}_{IU}\boldsymbol{h}_{IU}^H\boldsymbol{x}\right) \le 0, \tag{16}$$
$$\text{tr}\left(v_2 - \frac{1}{\sigma_e^2}\boldsymbol{x}^H\boldsymbol{h}_{IE}\boldsymbol{h}_{IE}^H\boldsymbol{x}\right) \le 0. \tag{17}$$

The equations in (15)-(17) can be further transformed into a compact form

$$\text{tr}\left((\boldsymbol{x}-\boldsymbol{\Theta}\boldsymbol{G}_{AI}\boldsymbol{w})(\boldsymbol{x}-\boldsymbol{\Theta}\boldsymbol{G}_{AI}\boldsymbol{w})^H\right)+\text{tr}\left(v_1-\frac{1}{\sigma^2}\boldsymbol{x}^H\boldsymbol{h}_{IU}\boldsymbol{h}_{IU}^H\boldsymbol{x}\right) + \text{tr}\left(v_2 - \frac{1}{\sigma_e^2}\boldsymbol{x}^H\boldsymbol{h}_{IE}\boldsymbol{h}_{IE}^H\boldsymbol{x}\right) \le 0. \tag{18}$$

The proof is given in **Appendix** A. In (13) and (14), constraints are linear and convex. Based on **Theorem** 1, it is not difficult to find that constraint (18) is a standard DC form. Then, we replace (12b), (12c), and (12d) with (13), (14), and (18). Problem (12) can be rewritten as a DC programming problem

$$\max_{\boldsymbol{w},\boldsymbol{x},\{v_i\}_{i=1,2}} \ \ln(1+v_2)-\ln(1+v_1), \tag{19a}$$
$$\text{s.t. } \begin{bmatrix} v_1 & \boldsymbol{x}^H\boldsymbol{h}_{IU} \\ \boldsymbol{h}_{IU}^H\boldsymbol{x} & \sigma^2\boldsymbol{I} \end{bmatrix} \succeq \boldsymbol{0}, \tag{19b}$$
$$\begin{bmatrix} v_2 & \boldsymbol{x}^H\boldsymbol{h}_{IE} \\ \boldsymbol{h}_{IE}^H\boldsymbol{x} & \sigma_e^2\boldsymbol{I} \end{bmatrix} \succeq \boldsymbol{0}, \tag{19c}$$
$$\text{tr}\left((\boldsymbol{x}-\boldsymbol{\Theta}\boldsymbol{G}_{AI}\boldsymbol{w})(\boldsymbol{x}-\boldsymbol{\Theta}\boldsymbol{G}_{AI}\boldsymbol{w})^H\right) + \text{tr}\left(v_1 - \frac{1}{\sigma^2}\boldsymbol{x}^H\boldsymbol{h}_{IU}\boldsymbol{h}_{IU}^H\boldsymbol{x}\right) + \text{tr}\left(v_2 - \frac{1}{\sigma_e^2}\boldsymbol{x}^H\boldsymbol{h}_{IE}\boldsymbol{h}_{IE}^H\boldsymbol{x}\right) \le 0, \tag{19d}$$
$$\text{tr}\left(\boldsymbol{w}\boldsymbol{w}^H\right) \le P_s, \tag{19e}$$
$$|\theta_n| = 1, n = 1, \cdots, N_r. \tag{19f}$$

To cope with the problem in (19), an alternating optimization algorithm is proposed for solving problem (19). Next, we firstly use manifold optimization to deal with the constraint condition in (19f).

B. MANIFOLD OPTIMIZATION ALGORITHM

To simplify the expression of the problem in (19), we define the functions as follows

$$f(v_2) = \ln(1+v_2), \tag{20}$$
$$h(\boldsymbol{w},\boldsymbol{\Theta},\boldsymbol{x}) = \text{tr}\left(\frac{1}{\sigma^2}\boldsymbol{x}^H\boldsymbol{h}_{IU}\boldsymbol{h}_{IU}^H\boldsymbol{x}\right) + \text{tr}\left(\frac{1}{\sigma_e^2}\boldsymbol{x}^H\boldsymbol{h}_{IE}\boldsymbol{h}_{IE}^H\boldsymbol{x}\right). \tag{21}$$

Employing the exact penalty method [35], (19) can be rewritten as

$$\min_{\boldsymbol{w},\boldsymbol{\Theta},\boldsymbol{x},v_i} \ f(v_2)-\ln(1+v_1) + \lambda(v_1+v_2+\|\boldsymbol{x}-\boldsymbol{\Theta}\boldsymbol{G}_{AI}\boldsymbol{w}\|^2 - h(\boldsymbol{w},\boldsymbol{\Theta},\boldsymbol{x})), \tag{22a}$$
$$\text{s.t. (19b)} - \text{(19f)}, \tag{22b}$$

where $\lambda > 0$ is a sufficiently large weight. Since (19f) is non-convex, problem (22) is difficult to solve for traditional methods. Hence, we adopt the alternating optimization algorithm and divide (22) into two subproblems, i.e.

$$\min_{\boldsymbol{\Theta}} \ f(\bar{v}_2)-\ln(1+\bar{v}_1)+\lambda\big(\bar{v}_1+\bar{v}_2 \|\boldsymbol{x}-\boldsymbol{\Theta}\boldsymbol{G}_{AI}\boldsymbol{w}\|^2 - h(\bar{\boldsymbol{w}},\boldsymbol{\Theta},\bar{\boldsymbol{x}})\big), \tag{23a}$$
$$\text{s.t. (19f)}. \tag{23b}$$

and

$$\min_{\boldsymbol{w},x,\{v_i\}_{i=1,2}} \ f(v_2)-\ln(1+v_1)+\lambda\big(v_1+v_2 + \|\boldsymbol{x}-\boldsymbol{\Theta}\boldsymbol{G}_{AI}\boldsymbol{w}\|^2 - h\left(\boldsymbol{w},\bar{\boldsymbol{\Theta}},\boldsymbol{x}\right)\big), \tag{24a}$$
$$\text{s.t. (19b), (19c), (19e)}, \tag{24b}$$

where $\bar{\boldsymbol{x}}, \bar{\boldsymbol{w}}, \bar{v}_i, \bar{\boldsymbol{\Theta}}$ are fixed values. We use manifold optimization technology to resolve problem (23). Based on the notion of manifold optimization, (23) is denoted as

$$\min_{\mathcal{M}} \ f(\bar{v}_2)-\ln(1+\bar{v}_1) + \lambda\big(\bar{v}_1+\bar{v}_2\|\boldsymbol{x}-\boldsymbol{\Theta}\boldsymbol{G}_{AI}\boldsymbol{w}\|^2 - h(\bar{\boldsymbol{w}},\boldsymbol{\Theta},\bar{\boldsymbol{x}})\big), \tag{25}$$

where $\mathcal{M}$ is the manifold space defined in the unit-modulus constraints in (23b) and $\mathcal{M}$ is expressed as

$$\mathcal{M} = \left\{\boldsymbol{\theta} \in \mathbb{C}^{N_r\times 1} \,||\, |\theta_1| = \cdots = |\theta_{N_r}| = 1\right\}. \tag{26}$$

Algorithm 1 Proposed Manifold Optimization Algorithm for Problem (23)

1 **Initialization:** $t = 0$, $\boldsymbol{\Theta}^{(t)} = \hat{\boldsymbol{\Theta}}$, accuracy ϵ.
2 **Repeat:**
3 Calculate the Euclidean gradient based on (28) ;
4 Update the Riemannian gradient based on (29) ;
5 Determine the step size $\delta^{(t+1)}$ based on [34] ;
6 Perform gradient descent algorithm over the current tangent space using $\boldsymbol{\theta}^{(t)} - \delta \nabla_{\boldsymbol{\theta}^{(t)}} f(\boldsymbol{\theta}^{(t)})$;
7 Update $\Theta^{(t+1)}$ according to (30) ;
8 Set $t = t + 1$;
9 **Until:** $\|\boldsymbol{\theta}^{(t+1)} - \boldsymbol{\theta}^{(t)}\| \leq \epsilon$.
10 **Output:** The optimal solution $\boldsymbol{\Theta}^*$.

The principle of manifold optimization method is to operate the gradient descent algorithm in manifold space. It is not difficult to find that gradient descent algorithm on Riemannian manifold is similar to that working in Euclidean space. But manifold optimization needs to calculate the Riemannian gradient as search direction. The Riemannian gradient of (25) at the current point $\boldsymbol{\theta}$ is defined as a projection of search direction in Euclidean space onto the tangent space $\mathcal{T}_{\boldsymbol{\theta}}\mathcal{M}$, which can be expressed as

$$\mathcal{T}_{\boldsymbol{\theta}}\mathcal{M} = \left\{ \boldsymbol{u} \in \mathbb{C}^{N_r \times 1} | \mathrm{Re}\left\{ \boldsymbol{\theta}^H \odot \boldsymbol{u} \right\} = 0 \right\}. \tag{27}$$

Then, the Euclidean gradient of (25) at $\boldsymbol{\theta}$ can be computed by

$$\nabla_{\boldsymbol{\theta}} f(\boldsymbol{\theta}) = \begin{bmatrix} \left(\mathbf{I} \odot \left(\boldsymbol{G}_{AI} \bar{\boldsymbol{w}} \bar{\boldsymbol{x}}^H\right)\right)_{1,1} \\ \vdots \\ \left(\mathbf{I} \odot \left(\boldsymbol{G}_{AI} \bar{\boldsymbol{w}} \bar{\boldsymbol{x}}^H\right)\right)_{N_r, N_r} \end{bmatrix}, \tag{28}$$

where $f(\boldsymbol{\theta}) = f(\bar{v}_2) - \ln(1+\bar{v}_1) + \lambda\big(\bar{v}_1 + \bar{v}_2 + \|\boldsymbol{x} - \boldsymbol{\Theta}\boldsymbol{G}_{AI}\boldsymbol{w}\|^2 - h(\bar{\boldsymbol{w}}, \boldsymbol{\Theta}, \bar{\boldsymbol{x}})\big)$. Based on the Euclidean gradient, the Riemannian gradient of (25) is expressed as

$$\mathrm{grad}_{\boldsymbol{\theta}} f(\boldsymbol{\theta}) = \nabla_{\boldsymbol{\theta}} f(\boldsymbol{\theta}) - \Re\{\nabla_{\boldsymbol{\theta}} f(\boldsymbol{\theta}) \odot \boldsymbol{\theta}\} \odot \boldsymbol{\theta}. \tag{29}$$

Thus, the current point $\boldsymbol{\theta}$ in the tangent space $\mathcal{T}_{\boldsymbol{\theta}}\mathcal{M}$ is updated by $\boldsymbol{\theta} - \delta \nabla_{\boldsymbol{\theta}} f(\boldsymbol{\theta})$, where $\delta > 0$ is the step size. It should be noticed that the update point may leave the manifold space. Thus, a retraction operation is used to make the point stay in the manifold. Finally, the retraction operation is expressed as

$$\mathrm{Ret}(\delta \nabla_{\boldsymbol{\theta}} f(\boldsymbol{\theta})) = \frac{\boldsymbol{\theta} - \delta \nabla_{\boldsymbol{\theta}} f(\boldsymbol{\theta})}{\|\boldsymbol{\theta} - \delta \nabla_{\boldsymbol{\theta}} f(\boldsymbol{\theta})\|}. \tag{30}$$

Via these operations, we can get the solution $\boldsymbol{\theta}^*$ and $\boldsymbol{\Theta}^* = \mathrm{diag}(\boldsymbol{\theta}^*)$. The details are summarised in **Algorithm** 1. Because **Algorithm** 1 is a gradient descent algorithm, in each iteration, the (25) is monotonically decreasing. Hence, **Algorithm** 1 will converge to a stationary point of (25) [34].

C. SCA-BASED OPTIMIZATION ALGORITHM

In this subsection, we optimize the $\boldsymbol{w}$, $\boldsymbol{x}$, and v_i when $\boldsymbol{\Theta} = \bar{\boldsymbol{\Theta}}$. (24a) is a standard DC programming problem. However, it is still non-convex. To deal with the non-convex objective function, we use the SCA method in [35] to transform the non-convex part of the objective function into a convex function, and then iteratively solve the convex approximation problem. In the following, we focus on finding the convex bounds of the concave functions $f(v_2)$ and $-h(\boldsymbol{w}, \bar{\boldsymbol{\Theta}}, \boldsymbol{x})$. We give the first-order Taylor expansion on point $(\bar{\boldsymbol{w}}, \bar{\boldsymbol{x}}, \bar{v}_2)$, and they are written as

$$\bar{f}(v_2|\bar{v}_2) = \ln(1+\bar{v}_2) + (1+\bar{v}_2)^{-1}(v_2 - \bar{v}_2), \tag{31}$$

$$\begin{aligned} -\bar{h}\left(\boldsymbol{w}, \bar{\boldsymbol{\Theta}}, \boldsymbol{x} | \bar{\boldsymbol{w}}, \bar{\boldsymbol{x}}\right) = & -\frac{1}{\sigma^2}\mathrm{tr}\left(\bar{\boldsymbol{x}}^H \boldsymbol{h}_{IU}\boldsymbol{h}_{IU}^H \bar{\boldsymbol{x}}\right) \\ & - 2\frac{1}{\sigma^2}\mathrm{Re}\left\{\mathrm{tr}\left(\bar{\boldsymbol{x}}^H \boldsymbol{h}_{IU}\boldsymbol{h}_{IU}^H (\boldsymbol{x} - \bar{\boldsymbol{x}})\right)\right\} \\ & - \frac{1}{\sigma_e^2}\mathrm{tr}\left(\bar{\boldsymbol{x}}^H \boldsymbol{h}_{IE}\boldsymbol{h}_{IE}^H \bar{\boldsymbol{x}}\right) \\ & - 2\frac{1}{\sigma_e^2}\mathrm{Re}\left\{\mathrm{tr}\left(\bar{\boldsymbol{x}}^H \boldsymbol{h}_{IE}\boldsymbol{h}_{IE}^H (\boldsymbol{x} - \bar{\boldsymbol{x}})\right)\right\}. \end{aligned} \tag{32}$$

It is not difficult to find that the first-order Taylor expansions of (20) and (21) are the linear function, and they are convex. Since $f(v_2)$ and $-h(\boldsymbol{w}, \bar{\boldsymbol{\Theta}}, \boldsymbol{x})$ are concave, according to [35], we obtain convex upper bounds of $f(v_2)$ and $-h(\boldsymbol{w}, \bar{\boldsymbol{\Theta}}, \boldsymbol{x})$ as

$$f(v_2) \leq \bar{f}(v_2|\bar{v}_2), \tag{41}$$

$$-h(\boldsymbol{w}, \bar{\boldsymbol{\Theta}}, \boldsymbol{x}) \leq -\bar{h}\left(\boldsymbol{w}, \bar{\boldsymbol{\Theta}}, \boldsymbol{x} | \bar{\boldsymbol{w}}, \bar{\boldsymbol{x}}\right). \tag{42}$$

Therefore, we have the following convex approximate problem

$$\begin{aligned} \min_{\boldsymbol{w}, \mathbf{X}, \{v_i\}_{i=1,2}} \ & \bar{f}(v_2|\bar{v}_2) - \ln(1+v_1) + \lambda\big(v_1 + v_2 \\ & - \bar{h}\left(\boldsymbol{w}, \bar{\boldsymbol{\Theta}}, \boldsymbol{x} | \bar{\boldsymbol{w}}, \bar{\boldsymbol{x}}\right)\big), \end{aligned} \tag{43a}$$

$$\text{s.t.} \begin{bmatrix} v_1 & \boldsymbol{x}^H \boldsymbol{h}_{IU} \\ \boldsymbol{h}_{IU}^H \boldsymbol{x} & \sigma^2 \boldsymbol{I} \end{bmatrix} \succeq \mathbf{0}, \tag{43b}$$

$$\begin{bmatrix} v_2 & \boldsymbol{x}^H \boldsymbol{h}_{IE} \\ \boldsymbol{h}_{IE}^H \boldsymbol{x} & \sigma_e^2 \boldsymbol{I} \end{bmatrix} \succeq \mathbf{0}, \tag{43c}$$

$$\mathrm{tr}\left(\boldsymbol{w}\boldsymbol{w}^H\right) \leq P_s. \tag{43d}$$

Selecting a point that satisfies the constraints of the problem (22), then the proposed SCA algorithm solve problem (43) in each iteration. The proposed SCA algorithm for problem (43) is summarized in **Algorithm** 2.

Algorithm 2 Proposed SCA-Based Algorithm for Problem (43)

1 **Initialization:** $t = 0$, $\bar{\boldsymbol{w}}^{(t)} = \bar{\boldsymbol{w}}^{(0)}$, $\bar{\boldsymbol{x}}^{(t)} = \bar{\boldsymbol{x}}^{(0)}$, $\bar{v}_i^{(t)} = \bar{v}_i^{(0)}$, accuracy ϵ_1.
2 **Repeat:**
3 Solving the convex problem (43) by using CVX [35] and the optimal solution is $\boldsymbol{w}^{(t+1)}$, $\boldsymbol{x}^{(t+1)}$, $v_i^{(t+1)}$
4 Set $t = t + 1$.
5 **Update:** $\bar{\boldsymbol{w}}^{(t+1)} = \boldsymbol{w}^*$, $\bar{\boldsymbol{x}}^{(t+1)} = \boldsymbol{x}^*$, $\bar{v}_i^{(t+1)} = v_i^*$.
6 **Until:** $\|\boldsymbol{w}^{(t+1)} - \boldsymbol{w}^{(t)}\| \leq \epsilon_1$.
7 **Output:** the optimal solution $\boldsymbol{w}^*$.

According to **Algorithm** 1 and **Algorithm** 2, the alternating optimization algorithm for problem (19) is summarized in **Algorithm** 3.

Algorithm 3 Proposed Alternating Optimization Algorithm for Problem (19)

1 **Initialization:** $t=0$, $\bar{\boldsymbol{w}}^{(t)}=\bar{\boldsymbol{w}}^{(0)}$, $\bar{\boldsymbol{x}}^{(t)}=\bar{\boldsymbol{x}}^{(0)}$, $\bar{v}_i^{(t)}=\bar{v}_i^{(0)}$, $\bar{\boldsymbol{\Theta}}^{(t)}=\bar{\boldsymbol{\Theta}}^{(0)}$
2 **Repeat:**
3 Executive the **Algorithm 1** to get $\boldsymbol{\Theta}^*$
4 Executive the **Algorithm 2** to get $\boldsymbol{w}^*$
5 **Until:** The objective function value is stable.
6 **Output:** the optimal solution $\boldsymbol{w}^*$ and $\boldsymbol{\Theta}^*$.

D. BEAMFORMING AND PHASE SHIFT OPTIMIZATION WITHOUT EAVESDROPPER'S CHANNEL

In this subsection, we consider the scenario when the eavesdropper's channel is unknown. Since the eavesdropper's channel is unknown, we cannot optimize the secrecy rate. To solve this problem, we adopt the AN-aided scheme in [24]. In this scheme, AP transmits AN to jam the eavesdropper. Therefore, the received signal at the IRS is expressed as

$$\tilde{\boldsymbol{r}}=\boldsymbol{\Theta}\boldsymbol{G}_{AI}\boldsymbol{w}s+\boldsymbol{\Theta}\boldsymbol{G}_{AI}\boldsymbol{z}, \tag{44}$$

where $\boldsymbol{z}\in\mathbb{C}^{N_t\times 1}$ is the AN. Then, the received signal at the user is denoted as

$$\tilde{y}=\boldsymbol{h}_{IU}^H\boldsymbol{\Theta}\boldsymbol{G}_{AI}\boldsymbol{w}s+\boldsymbol{h}_{IU}^H\boldsymbol{\Theta}\boldsymbol{G}_{AI}\boldsymbol{z}+n. \tag{45}$$

The received signal at the eavesdropper is expressed as

$$\tilde{y}_e=\boldsymbol{h}_{IE}^H\boldsymbol{\Theta}\boldsymbol{G}_{AI}\boldsymbol{w}s+\boldsymbol{h}_{IE}^H\boldsymbol{\Theta}\boldsymbol{G}_{AI}\boldsymbol{z}+n_e, \tag{46}$$

where $\boldsymbol{Z}=\mathbb{E}[\boldsymbol{z}\boldsymbol{z}^H]$ denotes the covariance matrix of $\boldsymbol{z}$. The achievable rate at the user is expressed as

$$\tilde{I}=\frac{1}{2}\log_2\left(1+\frac{\|\boldsymbol{h}_{IU}^H\boldsymbol{\Theta}\boldsymbol{G}_{AI}\boldsymbol{w}\|^2}{\boldsymbol{h}_{IU}^H\boldsymbol{\Theta}\boldsymbol{G}_{AI}\boldsymbol{Z}\boldsymbol{G}_{AI}^H\boldsymbol{\Theta}^H\boldsymbol{h}_{IU}+\sigma^2}\right). \tag{47}$$

The achievable rate at the eavesdropper is given by

$$\tilde{I}_e=\frac{1}{2}\log_2\left(1+\frac{\|\boldsymbol{h}_{IE}^H\boldsymbol{\Theta}\boldsymbol{G}_{AI}\boldsymbol{w}\|^2}{\boldsymbol{h}_{IE}^H\boldsymbol{\Theta}\boldsymbol{G}_{AI}\boldsymbol{Z}\boldsymbol{G}_{AI}^H\boldsymbol{\Theta}^H\boldsymbol{h}_{IE}+\sigma_e^2}\right). \tag{48}$$

We hope that the achievable rate of user satisfies the minimum user rate requirement, the power in information transmission is minimized, and more power is used to transmit AN, further confusing potential eavesdropper to optimize security. Therefore, our objective is to maximize AN power under the transmit power constraint and minimum user rate constraint. The problem can be expressed as

$$\max_{\boldsymbol{w},\boldsymbol{\Theta},\boldsymbol{Z}}\ \mathrm{tr}(\boldsymbol{Z}) \tag{49a}$$
$$\text{s.t. } \mathrm{tr}\left(\boldsymbol{w}\boldsymbol{w}^H\right)\le P_s, \tag{49b}$$
$$\tilde{I}\ge\gamma, \tag{49c}$$
$$\boldsymbol{Z}\succeq\boldsymbol{0}, \tag{49d}$$
$$|\theta_n|=1, n=1,\cdots,N_r. \tag{49e}$$

The optimization problem in (49) is also a non-convex problem, and the optimal solution is difficult to find. Similar to the problem in (12), The auxiliary variables $\boldsymbol{x}$, $\boldsymbol{Y}$, and u are introduced

$$\boldsymbol{x}=\boldsymbol{\Theta}\boldsymbol{G}_{AI}\boldsymbol{w}, \tag{50}$$
$$\boldsymbol{Y}=\boldsymbol{\Theta}\boldsymbol{G}_{AI}\boldsymbol{Z}\boldsymbol{G}_{AI}^H\boldsymbol{\Theta}^H, \tag{51}$$
$$u=\boldsymbol{x}_1^H\boldsymbol{h}_{IU}\left(\boldsymbol{h}_{IU}^H\boldsymbol{Y}_1\boldsymbol{h}_{IU}+\sigma^2\right)^{-1}\boldsymbol{h}_{IU}^H\boldsymbol{x}_1. \tag{52}$$

According to **Theorem** 1, we can equivalently transform (50), (51), and (52) into

$$\begin{bmatrix}u_1 & \boldsymbol{x}^H\boldsymbol{h}_{IU}\\ \boldsymbol{h}_{IU}^H\boldsymbol{x} & \boldsymbol{h}_{IU}^H\boldsymbol{Y}\boldsymbol{h}_{IU}+\sigma^2\end{bmatrix}\succeq\boldsymbol{0}, \tag{53}$$

$$\begin{aligned}&\mathrm{tr}\left(\left(\boldsymbol{Y}-\boldsymbol{\Theta}\boldsymbol{G}_{AI}\boldsymbol{Z}\boldsymbol{G}_{AI}^H\boldsymbol{\Theta}^H\right)\left(\boldsymbol{Y}^H-\boldsymbol{\Theta}\boldsymbol{G}_{AI}\boldsymbol{Z}\boldsymbol{G}_{AI}^H\boldsymbol{\Theta}^H\right)\right)\\&\quad+\mathrm{tr}\left((\boldsymbol{x}-\boldsymbol{\Theta}\boldsymbol{G}_{AI}\boldsymbol{w})(\boldsymbol{x}-\boldsymbol{\Theta}\boldsymbol{G}_{AI}\boldsymbol{w})^H\right)\\&\quad+\mathrm{tr}\left(u-\boldsymbol{x}^H\boldsymbol{h}_{IU}\left(\boldsymbol{h}_{IU}^H\boldsymbol{Y}\boldsymbol{h}_{IU}+\sigma^2\right)^{-1}\boldsymbol{h}_{IU}^H\boldsymbol{x}\right)\le 0.\end{aligned} \tag{54}$$

The third term of left hand side of (54) is convex and the proof is given in **Appendix** B. We define function $\tilde{h}(\boldsymbol{\Theta},\boldsymbol{x},u,\boldsymbol{Y},\boldsymbol{Z})$ as

$$\tilde{h}(\boldsymbol{\Theta},\boldsymbol{x},u,\boldsymbol{Y},\boldsymbol{Z})=+\mathrm{tr}\left(u-\boldsymbol{x}^H\boldsymbol{h}_{IU}\left(\boldsymbol{h}_{IU}^H\boldsymbol{Y}\boldsymbol{h}_{IU}+\sigma^2\right)^{-1}\boldsymbol{h}_{IU}^H\boldsymbol{x}\right). \tag{55}$$

Hence, employing the exact penalty method [35], problem (55) can be rewritten as

$$\begin{aligned}\min_{\boldsymbol{w},\boldsymbol{\Theta},\boldsymbol{Z},\boldsymbol{x},\boldsymbol{Y},u}\ &-\mathrm{tr}(\boldsymbol{Z})+\lambda(u+\|\boldsymbol{Y}-\boldsymbol{\Theta}\boldsymbol{G}_{AI}\boldsymbol{Z}\boldsymbol{G}_{AI}^H\boldsymbol{\Theta}^H\|^2\\&\quad+\|\boldsymbol{x}-\boldsymbol{\Theta}\boldsymbol{G}_{AI}\boldsymbol{w}\|^2-\tilde{h}(\boldsymbol{\Theta},x,u,\boldsymbol{Y},\boldsymbol{Z})),\end{aligned} \tag{56a}$$
$$\text{s.t. } \mathrm{tr}\left(\boldsymbol{w}\boldsymbol{w}^H\right)\le P_s, \tag{56b}$$
$$\tilde{I}\ge\gamma, \tag{56c}$$
$$\boldsymbol{Z}\succeq\boldsymbol{0}, \tag{56d}$$
$$|\theta_n|=1, n=1,\cdots,N_r. \tag{56e}$$
$$\begin{bmatrix}u & \boldsymbol{x}^H\boldsymbol{h}_{IU}\\ \boldsymbol{h}_{IU}^H\boldsymbol{x} & \boldsymbol{h}_{IU}^H\boldsymbol{Y}\boldsymbol{h}_{IU}+\sigma^2\end{bmatrix}\succeq\boldsymbol{0}, \tag{56f}$$

Similarly, we first optimize the phase shift matrix $\boldsymbol{\Theta}$ by resolving the following optimization problem

$$\min_{\mathcal{M}}-\mathrm{tr}(\hat{\boldsymbol{Z}})+\lambda\left(\mathrm{tr}(\hat{u})-\tilde{h}\left(\boldsymbol{\Theta},\hat{\boldsymbol{x}},\hat{u},\hat{\boldsymbol{Y}},\hat{\boldsymbol{Z}}\right)\right). \tag{57}$$

The Euclidean gradient of (57) is denoted as

$$\begin{aligned}\nabla_{\boldsymbol{\theta}}f(\boldsymbol{\theta})=&-\begin{bmatrix}(\boldsymbol{G}_{AI}\hat{\boldsymbol{w}}\hat{\boldsymbol{x}}^H)_{1,1}\\ \vdots\\ (\boldsymbol{G}_{AI}\hat{\boldsymbol{w}}\hat{\boldsymbol{x}}^H)_{N_r,N_r}\end{bmatrix}\\&-2\begin{bmatrix}(\Re\{\hat{\boldsymbol{Y}}^T\}\odot(\boldsymbol{G}_{AI}\hat{\boldsymbol{Z}}\boldsymbol{G}_{AI}^H))_{1,N_r}\\ \vdots\\ (\Re\{\hat{\boldsymbol{Y}}^T\}\odot(\boldsymbol{G}_{AI}\hat{\boldsymbol{Z}}\boldsymbol{G}_{AI}^H))_{N_r,1}\end{bmatrix},\end{aligned} \tag{58}$$

where $f(\boldsymbol{\theta})=-\mathrm{tr}\left(\hat{\boldsymbol{Z}}\right)+\lambda\left(\mathrm{tr}\left(\hat{u}\right)+\|\boldsymbol{Y}-\boldsymbol{\Theta}\boldsymbol{G}_{AI}\boldsymbol{Z}\boldsymbol{G}_{AI}^H\boldsymbol{\Theta}^H\|^2+\|\boldsymbol{x}-\boldsymbol{\Theta}\boldsymbol{G}_{AI}\boldsymbol{w}\|^2-\tilde{h}\left(\boldsymbol{\Theta},\hat{\boldsymbol{x}},\hat{u},\hat{\boldsymbol{Y}},\hat{\boldsymbol{Z}}\right)\right)$ and $\hat{u}$, $\hat{x}$, $\hat{\boldsymbol{Y}}$, and $\hat{\boldsymbol{Z}}$ are

Algorithm 4 Proposed Manifold Optimization Algorithm for Problem (23)

1 **Initialization:** $t = 0$, $\boldsymbol{\Theta}^{(t)} = \hat{\boldsymbol{\Theta}}$, accuracy ϵ_2.
2 **Repeat:**
3 Calculate the Euclidean gradient based on (58).
4 Update the Riemannian gradient based on (29).
5 Determine the step size $\delta^{(t+1)}$ based on [34].
6 Perform gradient descent algorithm over the current tangent space using $\boldsymbol{\theta}^{(t)} - \delta \nabla_{\boldsymbol{\theta}^{(t)}} f(\boldsymbol{\theta}^{(t)})$.
7 Update $\Theta^{(t+1)}$ according to (30).
8 Set $t = t + 1$.
9 **Until:** $\|\boldsymbol{\theta}^{(t+1)} - \boldsymbol{\theta}^{(t)}\| \leq \epsilon_2$.
10 **Output:** The optimal solution $\boldsymbol{\Theta}^*$.

fixed value. Then we can compute the tangent space, Riemannian gradient and retraction according to (29) and (30). The algorithm is summarized in **Algorithm** 4. In the following we optimize $\boldsymbol{w}, \boldsymbol{Z}, \boldsymbol{x}, \boldsymbol{Y}, u$ by setting $\Theta = \hat{\Theta}$ and the suboptimal problem is finally denoted as

$$\begin{aligned}
\min_{\boldsymbol{w},\boldsymbol{Z},\boldsymbol{x},\boldsymbol{Y},u} \quad & -\mathrm{tr}(\boldsymbol{Z}) + \lambda(u - \\
& \tilde{h}(\hat{\boldsymbol{\Theta}}, \boldsymbol{x}, u, \boldsymbol{Y}, \boldsymbol{Z}|\hat{\boldsymbol{\Theta}}, \hat{\boldsymbol{x}}, \hat{u}, \hat{\boldsymbol{Y}}, \hat{\boldsymbol{Z}})) && \text{(59a)} \\
\text{s.t.} \quad & \log(1+u) \geq \gamma && \text{(59b)} \\
& \mathrm{tr}\left(\boldsymbol{w}\boldsymbol{w}^H\right) \leq P_s, && \text{(59c)} \\
& \boldsymbol{Z} \succeq \boldsymbol{0}, && \text{(59d)} \\
& \begin{bmatrix} u_1 & \boldsymbol{x}^H\boldsymbol{h} \\ \boldsymbol{h}_{IU}^H\boldsymbol{x} & \boldsymbol{h}_{IU}^H\boldsymbol{Y}_1\boldsymbol{h}_{IU} + \sigma^2 \end{bmatrix} \succeq \boldsymbol{0}, && \text{(59e)}
\end{aligned}$$

where $\tilde{h}(\hat{\boldsymbol{\Theta}}, \boldsymbol{x}, u, \boldsymbol{Y}, \boldsymbol{Z}|\hat{\boldsymbol{\Theta}}, \hat{\boldsymbol{x}}, \hat{u}, \hat{\boldsymbol{Y}}, \hat{\boldsymbol{Z}})$ is Taylor series expansion and they are given by

$$\begin{aligned}
& -\tilde{h}\left(\hat{\boldsymbol{\Theta}}, x, \boldsymbol{Y}, \boldsymbol{w}, \boldsymbol{Z}|\hat{x}, \hat{\boldsymbol{Y}}, \hat{\boldsymbol{w}}, \hat{\boldsymbol{Z}}\right) \\
& = -\mathrm{tr}\left(\hat{x}^H\boldsymbol{h}_{IU}(\boldsymbol{h}_{IU}^H\hat{\boldsymbol{Y}}\boldsymbol{h}_{IU} + \sigma^2)^{-1}\boldsymbol{h}_{IU}^H\hat{x}\right) \\
& \quad + \mathrm{Re}\Bigg\{\mathrm{tr}\Bigg(\hat{x}^H\boldsymbol{h}_{IU}\left(\boldsymbol{h}_{IU}^H\hat{\boldsymbol{Y}}\boldsymbol{h}_{IU} + \sigma^2\right)^{-1}\left(\boldsymbol{Y} - \hat{\boldsymbol{Y}}\right) \\
& \qquad \left(\boldsymbol{h}_{IU}^H\hat{\boldsymbol{Y}}\boldsymbol{h}_{IU} + \sigma^2\right)^{-1}\boldsymbol{h}_{IU}^H\hat{x}\Bigg)\Bigg\} \\
& \quad - \mathrm{Re}\left\{\mathrm{tr}(\hat{x}^H\boldsymbol{h}_{IU}(\boldsymbol{h}_{IU}^H\hat{\boldsymbol{Y}}\boldsymbol{h}_{IU} + \sigma^2)^{-1}\boldsymbol{h}_{IU}^H(\hat{x} - x))\right\}. \qquad \text{(60)}
\end{aligned}$$

Then by using the proposed algorithm in the previous section, we can obtain the suboptimal solution of (59). The scheme is summarized in **Algorithm** 5. The numerical simulations are employed to evaluate the performance of the proposed algorithms in this article.

E. COMPUTATION COMPLEXITY

The computation complexity of the proposed **Algorithm** 3 and 6 are mainly from solving problems in (23), (24) and (57), (59). According to [40], the computation complexity of proposed algorithm for (24) and (59) are $(6N_t^2 + 4N_r^2 + 2N_tN_r)^{3.5}\log(1/\epsilon)$ and $(6N_t^2 + 4N_r^2 + 2N_tN_r)^{3.5}\log(1/\epsilon_3)$,

Algorithm 5 Proposed SCA-Based Alternating Optimization Algorithm for Problem (59)

1 **Initialization:** $t = 0$, $\boldsymbol{w}^{(t)} = \hat{\boldsymbol{w}}$, $\boldsymbol{x}_1^{(t)} = \hat{\boldsymbol{x}}_1$, $u_1^{(t)} = \hat{u}_1$, $\boldsymbol{Y}_1^{(t)} = \hat{\boldsymbol{Y}}_1$, accuracy ϵ_3.
2 **Repeat:**
3 Solving the convex problem (59) by using CVX [35] and the optimal solution is $\boldsymbol{w}^{(t+1)}$, $\boldsymbol{x}^{(t+1)}$, $u_1^{(t+1)}$, $\boldsymbol{Y}_1^{(t+1)}$.
4 Set $t = t + 1$.
5 **Update:** $\hat{\boldsymbol{w}} = \boldsymbol{w}^{(t+1)}$, $\hat{u}_1 = u_1^{(t+1)}$, $\hat{\boldsymbol{x}}_1 = \boldsymbol{x}_1^{(t+1)}$, $\hat{\boldsymbol{\Theta}} = \boldsymbol{\Theta}^{(t+1)}$, $\hat{\boldsymbol{Y}}_1 = \boldsymbol{Y}_1^{(t+1)}$.
6 **Until:** $\|\boldsymbol{w}^{(t+1)} - \boldsymbol{w}^{(t)}\| \leq \epsilon_3$.
7 **Output:** the optimal solution $\boldsymbol{w}^*$.

Algorithm 6 Proposed Alternating Optimization Algorithm for Problem (49)

1 **Initialization:** $t = 0$, $\bar{\boldsymbol{w}}^{(t)} = \bar{\boldsymbol{w}}^{(0)}$, $\bar{\boldsymbol{x}}^{(t)} = \bar{\boldsymbol{x}}^{(0)}$, $\bar{v}_i^{(t)} = \bar{v}_i^{(0)}$, $\bar{\boldsymbol{\Theta}}^{(t)} = \bar{\boldsymbol{\Theta}}^{(0)}$.
2 **Repeat:**
3 Executive the **Algorithm 4** to get $\boldsymbol{\Theta}^*$.
4 Executive the **Algorithm 5** to get $\boldsymbol{w}^*$.
5 **Until:** The objective function value is stable.
6 **Output:** the optimal solution $\boldsymbol{w}^*$ and $\boldsymbol{\Theta}^*$.

respectively, where ϵ and ϵ_3 are estimation accuracy. According to [34], the computation complexity of solving problem (23) and (57) is $I_{t1}(N_r^2N_t + N_r^2 + 2N_r)$ and $I_{t3}(N_r^3 + N_r^2N_t + N_t^2N_r + 2N_r)$, respectively, where I_{t1} and I_{t3} are the number of iterations of **Algorithm** 1 and 4. Therefore, the computation complexity of the proposed **Algorithm** 3 and 6 is

$$\begin{aligned}
\mathcal{O}(I_{t2}((6N_t^2 + 4N_r^2 + 2N_tN_r)^{3.5}\log(1/\epsilon) \\
+ I_{t1}(N_r^2N_t + N_r^2 + 2N_r))) \qquad \text{(61)}
\end{aligned}$$

and

$$\begin{aligned}
\mathcal{O}(I_{t4}((6N_t^2 + 4N_r^2 + 2N_tN_r)^{3.5}\log(1/\epsilon_3) \\
+ I_{t3}(N_r^3 + N_r^2N_t + N_t^2N_r + 2N_r))), \qquad \text{(62)}
\end{aligned}$$

where I_{t2} and I_{t4} are the number of iterations of **Algorithm** 3 and 6.

According to [43], the algorithm using the manifold optimization is guaranteed to converge to the point where the gradient of the objective function is 0. Therefore, **Algorithm** 1 and 4 ensure the decrease of the objective function and obtains a local optimal solution in each iteration. In addition, according to [35], the SCA algorithm also can converge to a stable point. Therefore, the alternating optimization algorithm converge.

IV. NUMERICAL RESULTS

In this section, we provide simulation results to validate the effectiveness of the proposed scheme. As shown in Fig.2, the AP, equipped with a ULA of $N_t = 16$ antennas, is located in the center of the IRS-aided mmWave system. The number of reflecting units of IRS $N_r = 16$. The distance between the

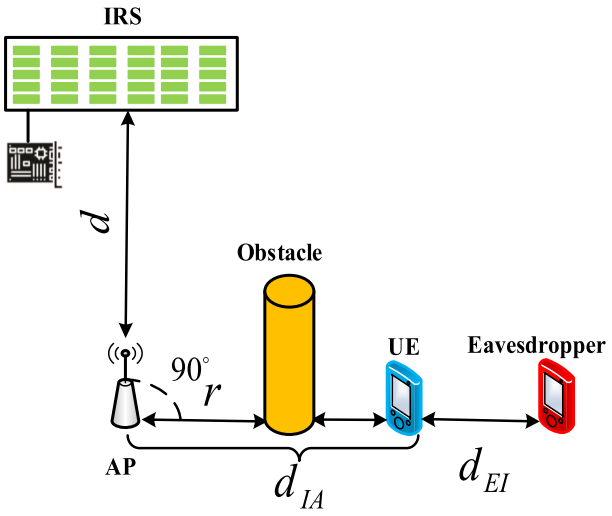

FIGURE 2. Deployment of IRS, user, Eavesdropper and EH receivers.

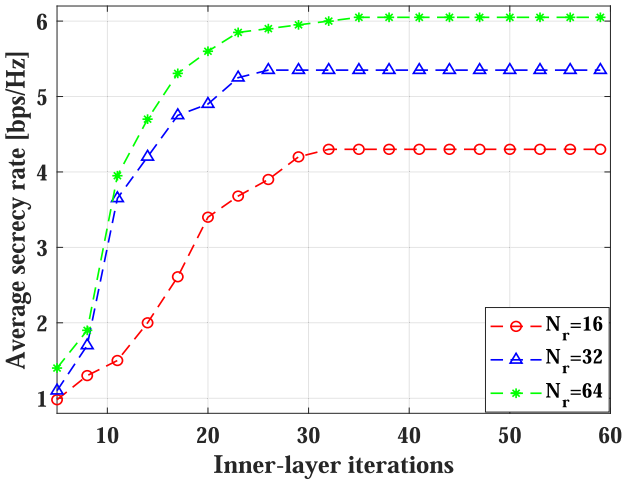

FIGURE 3. Convergence behaviour of the manifold optimization algorithm for problem (25).

AP and the obstacle $r = 10$ m. The distances between the eavesdropper and the UE, the AP and the IRS, the AP and the UE are respectively set to $d_{EI} = 20$ m, $d = 80$ m, and $d_{IA} = 100$ m. The transmit power is set as $P = 30$ dBm. In our simulations, the IRS-user and IRS-eavesdropper mmWave channel are generated according to the following geometric channel model [18]

$$\boldsymbol{h}_{IU} = \frac{1}{\sqrt{L_1}} \sum_{l=1}^{L_1} \alpha_l \boldsymbol{a}_I(\phi_l) \tag{63}$$

and

$$\boldsymbol{h}_{IE} = \frac{1}{\sqrt{L_2}} \sum_{l=1}^{L_2} \beta_l \boldsymbol{a}_E(\varphi_l) \tag{64}$$

where L_1 and L_2 are the number of paths, α_l and β_l are the complex gain associated with the lth path. According to [44]–[47], $\phi_l \in [0, 2\pi)$ and $\varphi_l \in [0, 2\pi)$ are the associated azimuth angle of departure. $\boldsymbol{a}_I$ and $\boldsymbol{a}_E$ are the array response vectors and they are respectively denoted as

$$\boldsymbol{a}_I(\phi_l) = \frac{1}{\sqrt{M}} \left[1, e^{\frac{j2\pi d \sin(\phi_l)}{\lambda}}, \ldots, e^{\frac{j(M-1)2\pi d \sin(\phi_l)}{\lambda}}\right]^T \tag{65}$$

and

$$\boldsymbol{a}_E(\varphi_l) = \frac{1}{\sqrt{M}} \left[1, e^{\frac{j2\pi d \sin(\varphi_l)}{\lambda}}, \ldots, e^{\frac{j(M-1)2\pi d \sin(\varphi_l)}{\lambda}}\right]^T, \tag{66}$$

where λ is the wavelength and $d = \frac{\lambda}{2}$ denotes the antenna spacing. The complex gains α_l and β_l are generated according to $\mathcal{CN}(0, 10^{-0.1PL(d)})$ [17], where $PL(d) = \eta_a + 10\eta_b \log_{10}(d) + \kappa$ is the log-normal shadowing variance, where $\eta_a = 72$, $\eta_b = 2.92$, $\sigma_\kappa = 8.7$ dB, and $\kappa \sim \mathcal{CN}(0, \sigma_\kappa^2)$. It is assumed that the IRS with N_r reflecting elements is installed on some high-rise buildings around the AP. Therefore, the LoS path is dominant for the AP-IRS mmWave channel and the rank-one channel model is adopted, i.e.,

$$\boldsymbol{G} = \gamma \boldsymbol{a}_r(\vartheta_1, \vartheta_2) \boldsymbol{a}_t^H(\varepsilon), \tag{67}$$

where $\vartheta_1 \in [0, 2\pi)$ and $\vartheta_2 \in [0, 2\pi)$ denote the azimuth angle of arrival and elevation angle of arrival associated with the BS-IRS path, respectively. $\varepsilon \in [0, 2\pi)$ is the associated angle of departure [47]. $\boldsymbol{a}_r(\vartheta_1, \vartheta_2)$ and $\boldsymbol{a}_t(\varepsilon)$ represent the receive and transmit array response vectors, respectively, where $\boldsymbol{a}_r(\vartheta_1, \vartheta_2)$ is denoted as

$$\boldsymbol{a}_r(\vartheta_1, \vartheta_2) = \boldsymbol{a}_x(\vartheta_2) \otimes \boldsymbol{a}_y(\vartheta_1), \tag{68}$$

where $\otimes$ stands for the Kronecker product. $\boldsymbol{a}_x(\vartheta_2)$ and $\boldsymbol{a}_y(\vartheta_1)$ are expressed as

$$\boldsymbol{a}_x(\vartheta_2) = \frac{1}{\sqrt{M_x}} \left[1, e^{\frac{j2\pi d \cos(\vartheta_2)}{\lambda}}, \ldots, e^{\frac{j(M_x-1)2\pi d \cos(\vartheta_2)}{\lambda}}\right]^T \tag{69}$$

and

$$\boldsymbol{a}_y(\vartheta_1) = \frac{1}{\sqrt{M_y}} \left[1, e^{\frac{j2\pi d \cos(\vartheta_1)}{\lambda}}, \ldots, e^{\frac{j(M_y-1)2\pi d \cos(\vartheta_1)}{\lambda}}\right]^T, \tag{70}$$

where M_x and M_y denote denote the number of antennas in the horizontal direction and the number of antennas in the vertical direction, respectively. $\boldsymbol{a}_t(\varepsilon)$ is denoted as

$$\boldsymbol{a}_t(\varepsilon) = \frac{1}{\sqrt{N_t}} \left[1, e^{\frac{j2\pi d \cos(\varepsilon)}{\lambda}}, \ldots, e^{\frac{j(N_t-1)2\pi d \cos(\varepsilon)}{\lambda}}\right]^T. \tag{71}$$

Similarly, the complex gain γ is generated according to $\mathcal{CN}(0, 10^{-0.1PL(d)})$, where $\eta_a = 61.4$, $\eta_b = 2$, and $\sigma_\kappa = 5.8$ dB. The noise power $\sigma_e^2 = \sigma^2 = -110$ dBm and the transmit power $P = 1$ W.

The convergence performance of the proposed algorithm is investigated. The iterations of the manifold optimization algorithm are termed as inner-layer iterations, and the iterations of the SCA-based algorithm are termed as the outer-layer iteration. In Fig. 3 and Fig. 4, we investigate the convergence behavior of the proposed algorithm with

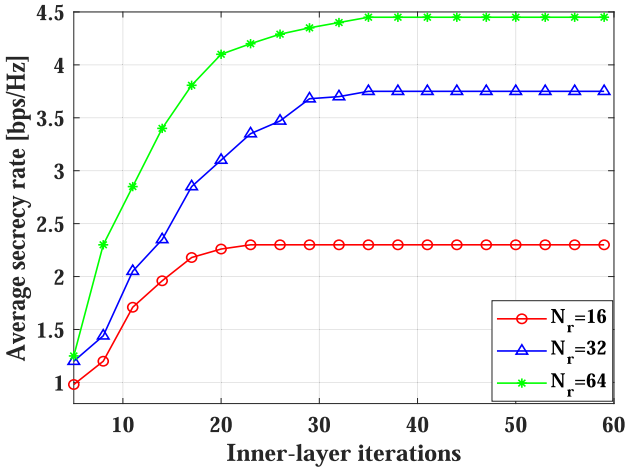

FIGURE 4. Convergence behaviour of the manifold optimization algorithm for problem (56).

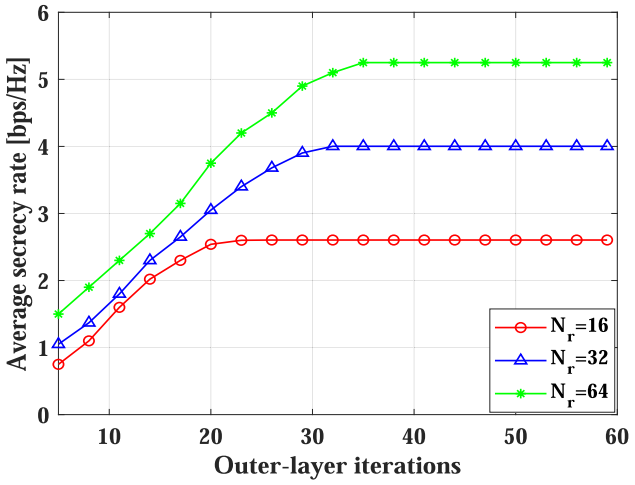

FIGURE 6. Convergence behaviour of the SCA-based algorithm for problem (57).

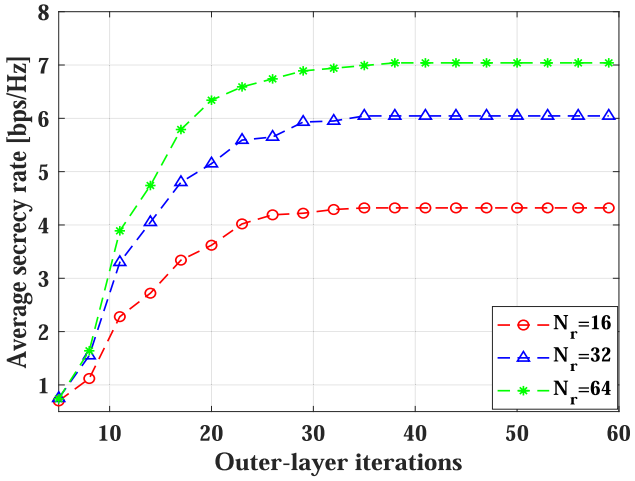

FIGURE 5. Convergence behaviour of the SCA-based algorithm for problem (43).

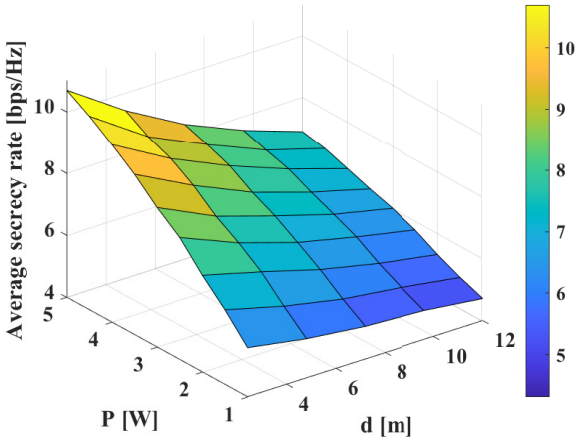

FIGURE 7. Average secrecy rate versus power P and distance d with eavesdropper's channel, $N_r = 16$.

versus the number of reflection elements N_r. It is observed that the average secrecy rate of the manifold optimization algorithm converges with the 25 iterations. The numerical results demonstrate the efficiency of the proposed algorithm. In addition, we find the slower convergence speed with more reflection elements. The reason is that more optimal variables bring heavier computation.

Fig. 5 and Fig. 6 show that the convergence performance of the SCA-based algorithm used for optimizing transmit beamforming. With the increase in the number of iterations, the secrecy rate increases and finally converges to a stable value. Similar to the inner-layer iteration, the convergence behavior of the outer-layer iteration can also get a similar conclusion, and the secrecy rate increases with the increase of the number of IRS phase shifts. In addition, it is not difficult to find that the SCA-based algorithm converges when the number of in the inner-layer iterations is about 30.

In Fig. 7 and Fig. 8, we evaluate the average secrecy rate as a function of the transmit power for various P and UE-to-eavesdropper distance d when the eavesdropper's CSI is unknown. In Fig. 7 and Fig. 8, with the decrease of P and the increase of distance d, the average secrecy rate increases. The main reason is that the more transmit power P will be used to suppress the eavesdropper. In addition, Fig. 7 and Fig. 8 also show that with the increase of the number of IRS phase shifts, the secrecy rate increases.

In Fig. 9, we evaluate the average secrecy rate as a function of the horizontal distance between the AP and user when the eavesdropper's CSI is unknown. These results demonstrate that the average secrecy rate gradually degrades with the decrease of the distance. It is because of high propagation loss caused by transmission between AP and the user that the reflected gain of IRS decreases a lot,which means only when the user adequately approaches IRS shall the reflected gain of IRS be easier to be utilized. Also, we observe that the proposed scheme outperforms the conventional algorithms. The reason is that, for the SCA scheme, the optimal objective is closer to the performance upper bound than others.

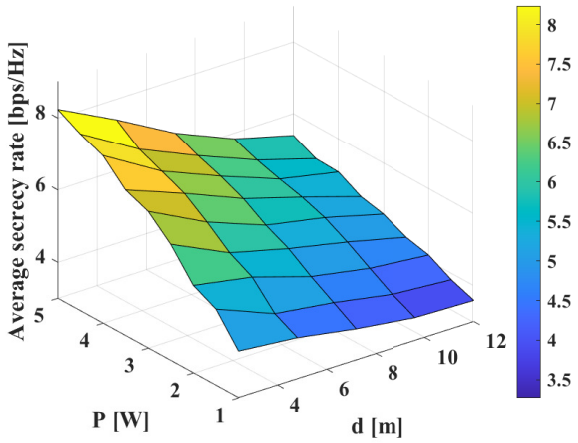

FIGURE 8. Average secrecy rate versus power P and distance d with eavesdropper's channel, $N_r = 8$.

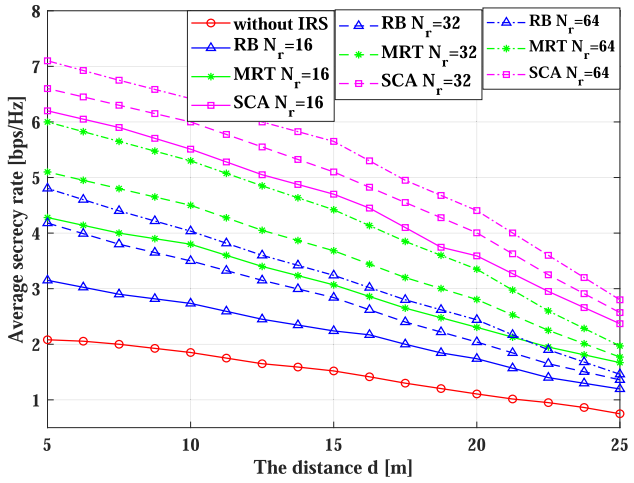

FIGURE 9. Average secrecy rate versus the distance between eavesdropper and user.

In addition, we see that the proposed IRS-aided mmWave system can achieve a higher average secrecy rate than the conventional mmWave system without IRS. This is because the phase shifts of the IRS are properly designed to enhance the received signal and suppress the eavesdropper. Finally, we find that the secrecy rate obviously increases with N_r. The result further confirms that more security improvement can be achieved by using a large IRS with more reflect elements.

In Fig.10, we investigate the transmit power on secrecy outage probability. Under different the number of phase shift of the IRS is plotted. The predefined threshold of achievable rate at the destination is $\gamma = 4$ bps/Hz. In Fig. 10, it is observed that when $\gamma = 4$ bps/Hz is fixed, as the increase of P, the secrecy outage probability of proposed scheme increases. This is because more power is allocated for AN from AP which reduces outage probability. It is not difficult to find when the transmit power is enough and the N_r is big enough, the proposed scheme can perfectly suppress the eavesdropper. The simulation results demonstrate that the IRS can get a good effect on achieving secrecy communication as well.

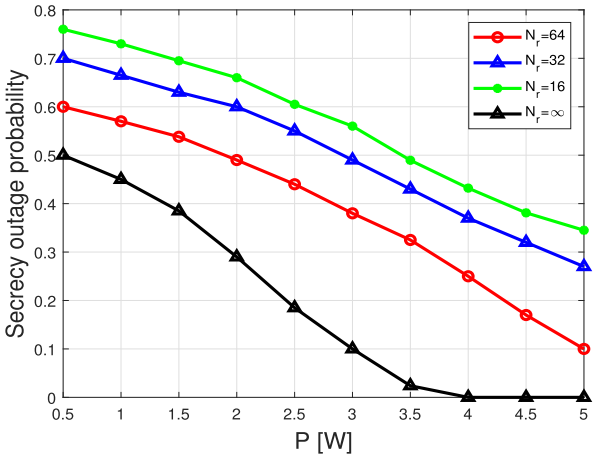

FIGURE 10. Secrecy outage probability versus the transmit power without eavesdropper's channel and $N_r = 16$.

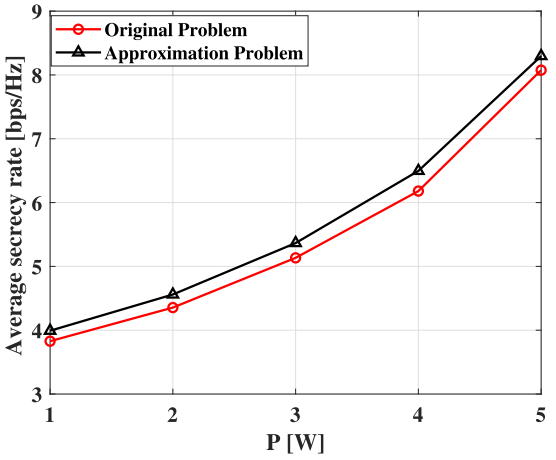

FIGURE 11. The gap between the convex approximation problem in (43) and the original problem in (26).

In Fig.11, we investigate the performance gap between the convex approximation problem in (43) and the original problem in (26). From Fig.11, It is not difficult to find that although we use a series of approximation operations to deal with the original problem, the performance gap between the convex approximation and original problem is small enough. The result demonstrates that the proposed approximation algorithm can achieve very good effect on secrecy communication.

V. CONCLUSION

We proposed alternating optimization algorithms for the IRS-aided mmWave system, i.e., the SCA and manifold optimization-based alternating optimization algorithm in this article. When the eavesdropper's channel is known, we transformed the original non-convex secrecy rate optimization problem into two sub-problems. First, we designed the phase shift of the IRS based on the manifold optimization algorithm. Then, given the phase shift matrix, we obtain the transmit beamforming of AP by exploiting the SCA algorithm. When the eavesdropper's channel is unknown, since

the secrecy rate can not be obtained, we use the AN-aided scheme by maximizing the AN power to suppress the eavesdropper under the minimum user rate requirement and transmit power constraints. Similarly, to resolve the AN power optimization problem, we proposed an SCA and manifold optimization-based alternating optimization algorithm. Finally, we analyzed the computation complexity of the proposed algorithms. Simulation results have shown that the IRS can improve the secrecy rate and proposed alternating optimization algorithms achieve higher secrecy rate than the conventional algorithms.

APPENDIX A
PROOF OF THEOREM 1

According to the Schur complement, $\begin{bmatrix} v_1 & x^H \boldsymbol{h}_{IU} \\ \boldsymbol{h}_{IU}^H x & \sigma^2 \boldsymbol{I} \end{bmatrix} \succeq \boldsymbol{0}$ and $\begin{bmatrix} v_2 & x^H \boldsymbol{h}_{IE} \\ \boldsymbol{h}_{IE}^H x & \sigma_e^2 \boldsymbol{I} \end{bmatrix} \succeq \boldsymbol{0}$ can be rewritten as

$$\begin{aligned} \mathrm{tr}\left(v_1 - \sigma^2 x^H \boldsymbol{h}_{IU} \boldsymbol{h}_{IU}^H x\right) &\geq 0, \\ \mathrm{tr}\left(v_2 - \sigma_e^2 x^H \boldsymbol{h}_{IE} \boldsymbol{h}_{IE}^H x\right) &\geq 0. \end{aligned} \tag{72}$$

Combining (72) with $\mathrm{tr}\left(v_1 - \sigma^2 x^H \boldsymbol{h}_{IU} \boldsymbol{h}_{IU}^H x\right) \leq 0$ and $\mathrm{tr}\left(v_2 - \sigma_e^2 x^H \boldsymbol{h}_{IE} \boldsymbol{h}_{IE}^H x\right) \leq 0$, Hence we have

$$\begin{aligned} \mathrm{tr}\left(v_1 - \frac{1}{\sigma^2} x^H \boldsymbol{h}_{IU} \boldsymbol{h}_{IU}^H x\right) &= 0, \\ \mathrm{tr}\left(v_2 - \frac{1}{\sigma_e^2} x^H \boldsymbol{h}_{IE} \boldsymbol{h}_{IE}^H x\right) &= 0. \end{aligned} \tag{73}$$

From (73), we have

$$v_1 = \frac{1}{\sigma^2} x^H \boldsymbol{h}_{IU} \boldsymbol{h}_{IU}^H x, \quad v_2 = \frac{1}{\sigma_e^2} x^H \boldsymbol{h}_{IE} \boldsymbol{h}_{IE}^H x. \tag{74}$$

Due to $\boldsymbol{x} = \boldsymbol{\Theta} \boldsymbol{G}_{AI} \boldsymbol{w}$, the $\|\boldsymbol{x} - \boldsymbol{\Theta} \boldsymbol{G}_{AI} \boldsymbol{w}\|^2 = 0$. Combine $\|\boldsymbol{x} - \boldsymbol{\Theta} \boldsymbol{G}_{AI} \boldsymbol{w}\|^2 = 0$ with $\mathrm{tr}(v_1 - \frac{1}{\sigma^2} \boldsymbol{x}^H \boldsymbol{h}_{IU} \boldsymbol{h}_{IU}^H \boldsymbol{x}) \leq 0$ and $\mathrm{tr}(v_2 - \frac{1}{\sigma_e^2} \boldsymbol{x}^H \boldsymbol{h}_{IE} \boldsymbol{h}_{IE}^H \boldsymbol{x}) \leq 0$, we have the constraint condition (18). In summary, **Theorem** 1 is proved.

APPENDIX B
PROOF OF THEOREM 2

We assume the function $f(\boldsymbol{Y}, \boldsymbol{x}_1) = \mathrm{tr}(\boldsymbol{x}_1^H \boldsymbol{h}_{IU} (\boldsymbol{h}_{IU}^H \boldsymbol{Y} \boldsymbol{h}_{IU} + \sigma^2)^{-1} \boldsymbol{h}_{IU}^H \boldsymbol{x}_1)$ and epigraph of $f(\boldsymbol{Y}, \boldsymbol{x}_1)$ is expressed as

$$\begin{aligned} \boldsymbol{epif} &= \Big\{(\boldsymbol{x}_1, \boldsymbol{Y}, t) | \boldsymbol{x}_1 \succeq \boldsymbol{0}, \\ &\qquad \mathrm{tr}\left(\boldsymbol{x}_1^H \boldsymbol{h}_{IU} (\boldsymbol{h}_{IU}^H \boldsymbol{Y} \boldsymbol{h}_{IU} + \sigma^2)^{-1} \boldsymbol{h}_{IU}^H \boldsymbol{x}_1\right) \leq t \Big\} \\ &= \Big\{(\boldsymbol{x}_1, \boldsymbol{Y}, t) | \boldsymbol{x}_1 \succeq \boldsymbol{0}, \mathrm{Vec}\left(\boldsymbol{x}_1^H \boldsymbol{h}_{IU}\right)^H \\ &\qquad \left(\left(\boldsymbol{h}_{IU}^H \boldsymbol{Y} \boldsymbol{h}_{IU} + \sigma^2\right)^{-T} \otimes \boldsymbol{I}\right) \mathrm{Vec}\left(\boldsymbol{x}_1 \boldsymbol{h}_{IU}^H\right) \leq t \Big\} \\ &= \Big\{(\boldsymbol{x}_1, \boldsymbol{Y}, t) | \boldsymbol{x}_1 \succeq \boldsymbol{0}, \\ &\qquad \begin{bmatrix} (\boldsymbol{h}_{IU}^H \boldsymbol{Y} \boldsymbol{h}_{IU} + \sigma^2)^{-1} \otimes \boldsymbol{I} & \mathrm{Vec}(\boldsymbol{Y}^H) \\ \mathrm{Vec}(\boldsymbol{Y}^H)^H & t \end{bmatrix} \succeq \boldsymbol{0} \Big\}. \end{aligned} \tag{75}$$

According to [35], the second equality is obtained based on $\mathrm{tr}(\boldsymbol{x}_1^H \boldsymbol{h}_{IU} (\boldsymbol{h}_{IU}^H \boldsymbol{Y} \boldsymbol{h}_{IU} + \sigma^2)^{-1} \boldsymbol{h}_{IU}^H \boldsymbol{x}_1) = \mathrm{Vec}(\boldsymbol{x}_1^H \boldsymbol{h}_{IU})^H ((\boldsymbol{h}_{IU}^H \boldsymbol{Y} \boldsymbol{h}_{IU} + \sigma^2)^{-T} \otimes \boldsymbol{I}) \mathrm{Vec}(\boldsymbol{x}_1 \boldsymbol{h}_{IU}^H)$, and based on Schur complement and identity $(\boldsymbol{A} \otimes \boldsymbol{B})^{-1} = \boldsymbol{A}^{-1} \otimes \boldsymbol{B}^{-1}$, we can obtain the third equality. The last equality of (75) is linear matrix inequality in $(\boldsymbol{x}_1, \boldsymbol{Y}, t)$, and therefore ***epif*** is convex, thus, $\mathrm{tr}(\boldsymbol{x}_1^H \boldsymbol{h}_{IU} (\boldsymbol{h}_{IU}^H \boldsymbol{Y} \boldsymbol{h}_{IU} + \sigma^2)^{-1} \boldsymbol{h}_{IU}^H \boldsymbol{x}_1)$.

REFERENCES

[1] Q. Wu and R. Zhang, "Towards smart and reconfigurable environment: Intelligent reflecting surface aided wireless network," *IEEE Commun. Mag.*, vol. 58, no. 1, pp. 106–112, Jan. 2020, doi: 10.1109/MCOM.001.1900107.

[2] Q. Wu and R. Zhang, "Intelligent reflecting surface enhanced wireless network: Joint active and passive beamforming design," in *Proc. IEEE Global Commun. Conf. (GLOBECOM)*, Abu Dhabi, United Arab Emirates, Dec. 2018, pp. 1–6.

[3] Q. Wu and R. Zhang, "Intelligent reflecting surface enhanced wireless network via joint active and passive beamforming," *IEEE Trans. Wireless Commun.*, vol. 18, no. 11, pp. 5394–5409, Nov. 2019.

[4] C. W. Huang, A. Zappone, D. Mérouane, and Y. Chau, "Achievable rate maximization by passive intelligent mirrors," in *Proc. IEEE Int. Conf. Acoust., Speech Signal Process. (ICASSP)*, Calgary, AB, Canada, Apr. 2018, pp. 3714–3718.

[5] C. Huang, A. Zappone, G. C. Alexandropoulos, M. Debbah, and C. Yuen, "Reconfigurable intelligent surfaces for energy efficiency in wireless communication," 2018, *arXiv:1810.06934*. [Online]. Available: http://arxiv.org/abs/1810.06934

[6] C. W. Huang, A. Zappone, D. Mérouane, and Y. Chau, "Beamforming optimization for intelligent reflecting surface with discrete phase shifts," in *Proc. IEEE Int. Conf. Acoust., Speech Signal Process. (ICASSP)*, Brighton, U.K., May 2019, pp. 7830–7833.

[7] C. W. Huang, A. Zappone, D. Mérouane, and Y. Chau, "Achievable rate maximization by passive intelligent mirrors," in *Proc. IEEE Globecom Workshops (GC Wkshps)*, Abu Dhabi, United Arab Emirates, Apr. 2018, pp. 1–6.

[8] C. Huang, A. Zappone, G. C. Alexandropoulos, M. Debbah, and C. Yuen, "Reconfigurable intelligent surfaces for energy efficiency in wireless communication," *IEEE Trans. Wireless Commun.*, vol. 18, no. 8, pp. 4157–4170, Aug. 2019.

[9] E. Björnson and L. Sanguinetti, "Power scaling laws and near-field behaviors of massive MIMO and intelligent reflecting surfaces," 2020, *arXiv:2002.04960*. [Online]. Available: http://arxiv.org/abs/2002.04960

[10] Z. Ding, R. Schober, and H. V. Poor, "On the impact of phase shifting designs on IRS-NOMA," 2020, *arXiv:2001.10909*. [Online]. Available: http://arxiv.org/abs/2001.10909

[11] X. Mu, Y. Liu, L. Guo, J. Lin, and N. Al-Dhahir, "Capacity and optimal resource allocation for IRS-assisted multi-user communication systems," 2020, *arXiv:2001.03913*. [Online]. Available: http://arxiv.org/abs/2001.03913

[12] C. Jia, H. Gao, N. Chen, and Y. He, "Machine learning empowered beam management for intelligent reflecting surface assisted mmWave networks," 2020, *arXiv:2003.01306*. [Online]. Available: http://arxiv.org/abs/2003.01306

[13] J. Yuan, X. Kong, Q. Wang, and C. Wu, "Intelligent radome design using multilayer metamaterial structures to realize energy isolation and asymmetric propagation of electromagnetic wave," 2020, *arXiv:2003.02594*. [Online]. Available: http://arxiv.org/abs/2003.02594

[14] Y. Zhang, C. J. Zhong, Z. Y. Zhang, and W. D. Lu, "Sum rate optimization for two way communications with intelligent reflecting surface," 2020, *arXiv:2003.02594*. [Online]. Available: http://arxiv.org/abs/2003.02594

[15] A. Taha, Y. Zhang, F. B. Mismar, and A. Alkhateeb, "Deep reinforcement learning for intelligent reflecting surfaces: Towards standalone operation," 2020, *arXiv:2002.11101*. [Online]. Available: http://arxiv.org/abs/2002.11101

[16] P. Wang, J. Fang, X. Yuan, Z. Chen, H. Duan, and H. Li, "Intelligent reflecting surface-assisted millimeter wave communications: Joint active and passive precoding design," 2019, *arXiv:1908.10734*. [Online]. Available: http://arxiv.org/abs/1908.10734

[17] P. L. Wang, J. Fang, and H. B. Li, "Joint beamforming for intelligent reflecting surface-assisted millimeter wave communications," 2019, *arXiv:1908.10734*. [Online]. Available: http://arxiv.org/abs/1908.10734

[18] A. Taha, M. Alrabeiah, and A. Alkhateeb, "Enabling large intelligent surfaces with compressive sensing and deep learning," 2019, *arXiv:1908.10734*. [Online]. Available: http://arxiv.org/abs/1908.10734

[19] A. Zappone, M. D. Renzo, and X. W. Qian, "Overhead-aware design of reconfigurable intelligent surfaces in smart radio environments," 2020, *arXiv:2003.02583*. [Online]. Available: http://arxiv.org/abs/2003.02583

[20] D. W. Yue, H. H. Nguyen, and Y. Sun, "Analysis of intelligent reflecting surface-assisted mmWave doubly massive-MIMO communications," 2020, *arXiv:2003.02583*. [Online]. Available: http://arxiv.org/abs/2003.02583

[21] C. Huang, R. Mo, C. Yuen, and S. Member, "Reconfigurable intelligent surface assisted multiuser MISO systems exploiting deep reinforcement learning," 2020, *arXiv:2002.10072*. [Online]. Available: http://arxiv.org/abs/2002.10072

[22] X. Yu, D. Xu, Y. Sun, D. W. K. Ng, and R. Schober, "Robust and secure wireless communications via intelligent reflecting surfaces," 2019, *arXiv:1912.01497*. [Online]. Available: http://arxiv.org/abs/1912.01497

[23] K. Feng and X. Li, "Physical layer security enhancement exploiting intelligent reflecting surface," 2019, *arXiv:1911.02766*. [Online]. Available: http://arxiv.org/abs/1911.02766

[24] B. Q. Feng, Y. P. Wu, and M. F. Zheng, "Secure transmission strategy for intelligent reflecting surface enhanced wireless system," in *Proc. 11th Int. Conf. Wireless Commun. Signal Process. (WCSP)*, Xi'an, China, Oct. 2019, pp. 1–6.

[25] M. Cui, G. Zhang, and R. Zhang, "Secure wireless communication via intelligent reflecting surface," *IEEE Wireless Commun. Lett.*, vol. 8, no. 5, pp. 1410–1414, Oct. 2019.

[26] D. Xu, X. Yu, Y. Sun, D. Wing Kwan Ng, and R. Schober, "Resource allocation for secure IRS-assisted multiuser MISO systems," 2019, *arXiv:1907.03085*. [Online]. Available: http://arxiv.org/abs/1907.03085

[27] J. Chen, Y.-C. Liang, Y. Pei, and H. Guo, "Intelligent reflecting surface: A programmable wireless environment for physical layer security," 2019, *arXiv:1905.03689*. [Online]. Available: http://arxiv.org/abs/1905.03689

[28] H. Shen, W. Xu, S. Gong, Z. He, and C. Zhao, "Secrecy rate maximization for intelligent reflecting surface assisted multi-antenna communications," 2019, *arXiv:1905.10075*. [Online]. Available: http://arxiv.org/abs/1905.10075

[29] W. Shi, X. Zhou, L. Jia, Y. Wu, F. Shu, and J. Wang, "Enhanced secure wireless information and power transfer via intelligent reflecting surface," 2019, *arXiv:1911.01001*. [Online]. Available: http://arxiv.org/abs/1911.01001

[30] X. Guan, Q. Wu, and R. Zhang, "Intelligent reflecting surface assisted secrecy communication: Is artificial noise helpful or not?" 2019, *arXiv:1907.12839*. [Online]. Available: http://arxiv.org/abs/1907.12839

[31] X. Guan, Q. Wu, and R. Zhang, "Intelligent reflecting surface assisted secrecy communication: Is artificial noise helpful or not?" *IEEE Wireless Commun. Lett.*, vol. 9, no. 6, pp. 778–782, Jan. 2020, doi: 10.1109/LWC.2020.2969629.

[32] X. Lu, W. Yang, X. Guan, Q. Wu, and Y. Cai, "Robust and secure beamforming for intelligent reflecting surface aided mmWave MISO systems," 2020, *arXiv:2003.11195*. [Online]. Available: http://arxiv.org/abs/2003.11195

[33] J. Qiao and M.-S. Alouini, "Secure transmission for intelligent reflecting surface-assisted mmWave and terahertz systems," 2020, *arXiv:2005.13451*. [Online]. Available: http://arxiv.org/abs/2005.13451

[34] P. A. Absil, R. Mahony, and R. Sepulchre, *Optimization Algorithms on Matrix Manifolds*. Princeton, NJ, USA: Princeton Univ. Press, 2009.

[35] S. Boyd and L. Vandenberghe, *Convex Optimization*. Cambridge, U.K.: Cambridge Univ. Press, 2004.

[36] P. Wang, J. Fang, H. Duan, and H. Li, "Compressed channel estimation and joint beamforming for intelligent reflecting surface-assisted millimeter wave systems," 2019, *arXiv:1911.07202*. [Online]. Available: http://arxiv.org/abs/1911.07202

[37] J. He, H. Wymeersch, L. Kong, O. Silvén, and M. Juntti, "Large intelligent surface for positioning in millimeter wave MIMO systems," 2019, *arXiv:1910.00060*. [Online]. Available: http://arxiv.org/abs/1910.00060

[38] J. G. He, W. Henk, S. Tachporn, S. Olli, and J. Markku, "Adaptive beamforming design for mmWave RIS-aided joint localization and communication," 2019, *arXiv:1911.02813*. [Online]. Available: http://arxiv.org/abs/1911.02813

[39] H. Guo, Y.-C. Liang, J. Chen, and E. G. Larsson, "Weighted sum-rate maximization for reconfigurable intelligent surface aided wireless networks," 2019, *arXiv:1912.11999*. [Online]. Available: http://arxiv.org/abs/1912.11999

[40] I. Pólik and T. Terlaky, "Interior point methods for nonlinear optimization," in *Nonlinear Optimization*, vol. 10, no. 3. Springer, Jun. 2016, pp. 215–276.

[41] W. Guo, A.-A. Lu, X. Meng, X. Gao, and N. Ma, "Broad coverage precoding design for massive MIMO with manifold optimization," *IEEE Trans. Commun.*, vol. 67, no. 4, pp. 2792–2806, Apr. 2019.

[42] X. Yu, J.-C. Shen, J. Zhang, and K. B. Letaief, "Alternating minimization algorithms for hybrid precoding in millimeter wave MIMO systems," *IEEE J. Sel. Topics Signal Process.*, vol. 10, no. 3, pp. 485–500, Apr. 2016.

[43] X. Yu, D. Xu, and R. Schober, "MISO wireless communication systems via intelligent reflecting surfaces," 2019, *arXiv:1904.12199*. [Online]. Available: http://arxiv.org/abs/1904.12199

[44] Y. Chen, D. Chen, Y. Tian, and T. Jiang, "Spatial lobes division-based low complexity hybrid precoding and diversity combining for mmWave IoT systems," *IEEE Internet Things J.*, vol. 6, no. 2, pp. 3228–3239, Apr. 2019.

[45] Y. Chen, D. Chen, and T. Jiang, "Non-uniform quantization codebook based hybrid precoding to reduce feedback overhead in millimeter wave MIMO systems," *IEEE Trans. Commun.*, vol. 67, no. 4, pp. 2779–2791, Apr. 2019.

[46] Y. Chen, D. Chen, T. Jiang, and L. Hanzo, "Millimeter-wave massive MIMO systems relying on generalized Sub-Array-Connected hybrid precoding," *IEEE Trans. Veh. Technol.*, vol. 68, no. 9, pp. 8940–8950, Sep. 2019.

[47] Y. Chen, D. Chen, T. Jiang, and L. Hanzo, "Channel-covariance and angle-of-departure aided hybrid precoding for wideband multiuser millimeter wave MIMO systems," *IEEE Trans. Commun.*, vol. 67, no. 12, pp. 8315–8328, Dec. 2019.

YUE XIU is currently pursuing the Ph.D. degree with the National Key Laboratory of Science and Technology on Communications, University of Electronic Science and Technology of China.

He joined the successive postgraduate and doctoral programs with the University of Electronic Science and Technology of China. In 2020, he became a Visiting Ph.D. Student at Nanyang Technology University (NTU). His research interests include convex optimization and millimeter communication systems.

ZHONGPEI ZHANG received the B.S. and M.S. degrees from the Physics Department, Sichuan Normal University, in 1990 and 1993, respectively, and the Ph.D. degree from the School of Computer and Communication Engineering, Southwest Jiaotong University, in 2000.

From 2001 to 2003, he was a Postdoctoral Fellow with the National Key Laboratory of Microwave and Digital Communication, Tsinghua University. From 2004 to 2005, he was a Postdoctoral Fellow with the University of Oulu. He is currently a Professor and the Ph.D. Tutor with the University of Electronic Science and Technology of China. He has authored or coauthored over 50 journal articles and conference papers. His research interests include channel coding, coordinated multiple points transmission, information theory, channel estimation, and so on.

Dr. Zhang is a Senior Member of the China Institute of Communications and a member of IEICE. He has participated in many research projects and chaired the National High-Tech Research and Development Program of China (863 Program) Coordinated Multiple Points Transmission and the National Natural Science Foundation of China Massive MIMO Channel Acquisition.